ORGANIC CHEMISTRY FRONTIERS

CCS 中国化学会 CHINESE CHEMICAL SOCIETY

SIOC 1950

ROYAL SOCIETY OF CHEMISTRY

RESEARCH ARTICLE

View Article Online
View Journal | View Issue

Cite this: *Org. Chem. Front.*, 2024, **11**, 7059

Single-bond-linked and vinylene-bridged azulenyl bis(squaraine) dyes: design, synthesis and molecular self-assembly behaviors†

Yiming Yao,[a] Hong Lin,[b] Shali Cai,[a] Xiaodi Yang *[b] and Xike Gao *[a]

Received 29th August 2024,
Accepted 28th September 2024

DOI: 10.1039/d4qo01604a

rsc.li/frontiers-organic

In this work, two azulenyl bis(squaraine) dyes were designed and synthesized, whose main structural difference lies in the connection model between two monomeric units. Their self-assembly behaviors were investigated in mixed solvents of different polarities, compound concentrations and temperatures. In particular, for the single-bond-linked squaraine dimer, J-aggregate nanosheets could be formed in a hexane system mixed with small amounts of tetrahydrofuran as a co-solvent. Meanwhile, additional absorption bands were observed in the second near-infrared (NIR-II, 1000–1700 nm) region for vinylene-bridged bis(squaraine) aggregates, elucidating the impact of the spacer unit on interchromophoric interaction modes. Moreover, in comparison with the monomer compound, organic field-effect transistor and morphological characterizations revealed that dimerization has a significant influence on the charge carrier mobility and thermal responsiveness of film aggregates. This study provides a promising chemical modification approach to improve assembly behavior and optoelectronic performance.

Introduction

Organic dyes with near-infrared (NIR) absorption/emission, such as perylene diimide,[1] porphyrin[2] and squaraine, can be applied in various fields, including organic photovoltaics and phototheranostics. Among them, squaraine is a type of zwitterionic dye produced *via* the condensation reactions between squaric acid or its derivatives and nucleophiles.[3] Thus, unsymmetrical squaraines are endowed with "D–A–D'" (D: donor; A: acceptor) structural features. Self-assembly behaviors of squaraines have gained widespread attention since aggregate structures can further affect their physicochemical properties and device performances.[4–7]

Bis(squaraine) dyes can be regarded as those involving intramolecular *J*-coupling of monomeric squaraine chromophores.[8] Subsequently, bis(squaraine) dyes can self-assemble into different aggregate structures, which may not be observed for monomeric squaraine dyes.[9] According to the literature, the intermolecular *J*-coupling effect can lead to the bathochromic shift of absorption bands,[10] while the formation of H-molecular aggregates is manifested as hypsochromic absorbance shifts, thereby inducing new properties.[11] For instance, F. Würthner *et al.*[12] and C. J. Collison *et al.*[13] reported that intermolecular charge transfer (ICT) interactions were observed in H-type bis(squaraine) aggregates except for the Coulomb coupling effect, resulting in additional new peaks in the long-wavelength region.

Moreover, bis-chromophores can be either directly linked or bridged *via* spacer units,[14–16] which presumably affects the arrangement of transition dipole moments and molecular packing structures. For example, Z. Liu *et al.*[17] and E. Hao *et al.*[18] revealed that vinylene-bridged chromophore dimers were appropriate molecular scaffolds to generate J-aggregates. As a result, alternating connection modes impacted the functional properties of NIR dyes.

Most of the reported bis(squaraine) compounds are connected through benzenoid moieties such as indolenine[19] and benzothiazole,[20] and those linked *via* nonbenzenoid segments are rarely investigated. As an isomer of naphthalene, azulene has a chemical structure composed of an electron-rich pentagon ring and electron-deficient heptagon ring, leading to a large dipole moment of 1.08 D.[21] The dipole orientation variations of azulene units in compounds have a major influence on molecular packing motifs and corresponding optoelectronic characteristics.[22,23] Moreover,

[a]*State Key Laboratory of Organometallic Chemistry, Shanghai Institute of Organic Chemistry, University of Chinese Academy of Sciences, Chinese Academy of Sciences, Shanghai 200032, P.R. China. E-mail: gaoxk@mail.sioc.ac.cn*
[b]*Innovation Research Institute of Traditional Chinese Medicine, Shanghai University of Traditional Chinese Medicine, Shanghai 201203, P. R. China. E-mail: yangxiaodi@shutcm.edu.cn*

† Electronic supplementary information (ESI) available. See DOI: https://doi.org/10.1039/d4qo01604a

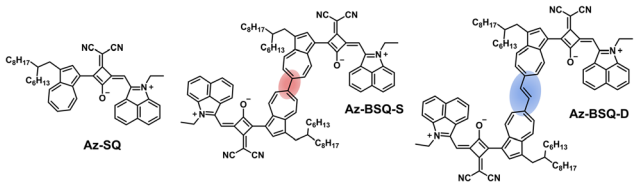

Fig. 1 Chemical structures of **Az-SQ**, **Az-BSQ-S** and **Az-BSQ-D**.

the azulene unit can be incorporated into a squaraine backbone at position 1/3, yielding azulenyl squaraines as photothermal transduction agents,[24] organic semiconducting materials,[25] *etc*.

In addition to structural modifications, the aggregate structures of NIR dyes can be modulated by changing the surrounding environment (*e.g.*, solvent polarity,[26] temperature[27] and additives[28]). Therefore, we designed and synthesized two bis(squaraine) compounds, namely, **Az-BSQ-S** and **Az-BSQ-D**, in which monomeric moieties (**Az-SQ**) were connected at the 6-position of an azulene unit *via* a single bond and a vinylene unit, respectively (Fig. 1). Self-assembly behavior studies were conducted in two systems of mixed solvents with different fractions, dye concentrations and temperatures. The results revealed that **Az-BSQ-D** nanoparticles could produce NIR-II absorption in addition to blue-shifted absorption peaks. Then, organic field-effect transistor (OFET) characterizations implied the effect of dimerization on the charge transport capability and thermal responsiveness of spin-coated films. Our work provides simple but effective approaches to fine-tune the intra- and intermolecular interactions of squaraine dyes, and will contribute to their application studies.

Results and discussion

Design and synthesis

The strong electron acceptor benz[*cd*]indolium[29,30] was used to construct a D–A–D′ squaraine unit. The synthesis routes of two bis(squaraine) dyes are depicted in Scheme 1. Starting from 6-bromoazulene, the Friedel–Crafts acylation reaction was carried out with 2-hexyldecanoyl chloride at the 1-position of the azulene unit[31] to give **2** in a yield of 48%. Then, a reduction reaction was realized to afford **3** in a yield of 60%. The grafted alkyl chain could not only promote the solubility of target compounds but also cut down the side reactions through the blocking of reactive 1-position. The nucleophilic reaction between **3** and squaryl dichloride produced compound **4** in a yield of 54%. Afterwards, the introduction of a dicyanomethylene (diCN) segment was accomplished through two steps[32] to obtain **6**, and the total yield was as high as 89%. Then, the condensation reaction between **6** and benz[*cd*]indolium derivative (**7**) afforded bromine-substituted squaraine **8** as a key intermediate in a yield of 76%. Finally, **Az-BSQ-S** and **Az-BSQ-D** were produced from compound **8** *via* Stille coupling reactions by using hexabutylditin[33] and bis(tributylstannyl)

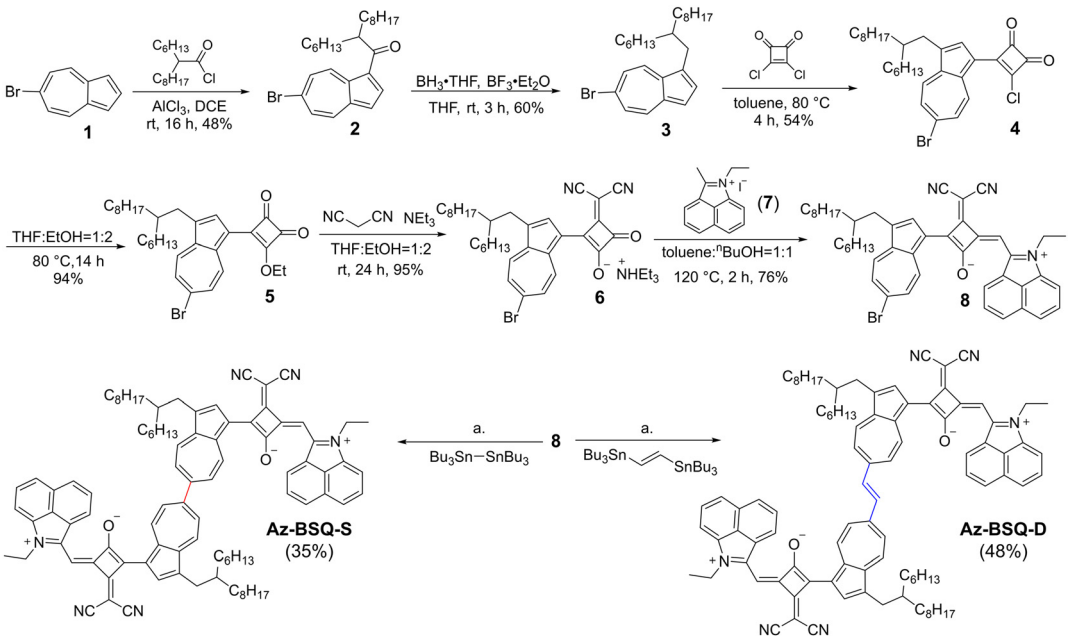

Scheme 1 Synthesis routes for **Az-BSQ-S** and **Az-BSQ-D**. Condition a. $Pd_2(dba)_3$, P(*o*-tol)$_3$, toluene, 110 °C, and 24 h.

ethene[34] as starting materials in yields of 35% and 48%, respectively.

To obtain the monomer **Az-SQ**, we first tried several [Pd]-catalyzed and ^{n}BuLi-involved reactions based on the intermediate **8** with different proton suppliers but failed.[35–37] Thereby, as shown in Scheme S1,† azulene was used to undergo synthetic reactions *via* similar routes depicted in Scheme 1 to afford **Az-SQ** in six steps. All the new compounds were characterized by ^{1}H NMR, ^{13}C NMR and high-resolution mass spectra.

Theoretical calculations

To examine the effect of the connection model on the geometries of the **Az-SQ** derivatives, molecular structure optimization, frontier molecular orbitals and dipole moments were calculated at DFT/B3LYP/6-31G(d,p) using the Gaussian 16 program[38] (to reduce the time required, the hexyldecyl chain was replaced with an isobutyl chain). For **Az-SQ**, the squaryl ring and benzindolium cycle were arranged in a coplanar way, while the dihedral angle between the azulene unit and four-membered ring was about 20° (Fig. S1†). The electron density of the highest occupied molecular orbital (HOMO) was distributed over the molecular skeleton and mainly localized on the central squaryl ring and azulene unit. The electron density of the lowest unoccupied molecular orbital (LUMO) was delocalized on the conjugated skeleton except the diCN substituents. The HOMO/LUMO energy levels and energy gap ($E_{HOMO-LUMO}$) of **Az-SQ** were calculated to be −4.80 eV/−3.19 eV and 1.61 eV, respectively. Moreover, the dipole moment direction of **Az-SQ** is shown in Fig. S1† and its value (μ) was 8.40 D.

Then, the DFT calculation results of **Az-BSQ-S** and **Az-BSQ-D** are illustrated in Fig. 2. **Az-BSQ-S** and **Az-BSQ-D** presented different dipole moment orientations, and their values were 2.14 D and 10.32 D, respectively. Such discrepancy in molecular dipole moments could lead to disparate self-assembly behaviors for two bis(squaraine) compounds under the effect of dipole–dipole interactions.[39] The torsion angle between the two monomeric units in **Az-BSQ-S** and **Az-BSQ-D** was about 50° and 44°, respectively, indicating the alleviation of steric hindrance between the seven-membered ring in the vinylene-bridged squaraine dimers.[40] Besides, two bis(squaraine) dyes exhibited varying frontier molecular orbital distributions. For **Az-BSQ-S**, the electron densities of HOMO and LUMO were concentrated more on one of the monomer units. For **Az-BSQ-D**, the electron density of LUMO was uniformly delocalized along the conjugated structure; however, the electron density of HOMO was localized on one monomeric segment. Compared with **Az-SQ**, the E_{HOMO} values of two bis(squaraine) dyes were lowered by 0.13 eV and E_{LUMO} values were lowered by about 0.1 eV. **Az-BSQ-S** and **Az-BSQ-D** possessed comparative HOMO–LUMO energy gaps of 1.58 eV and 1.55 eV, respectively. In addition, the simulated absorption spectra were acquired through time-dependent density functional theory (TD-DFT) calculations. As shown in Fig. S2,† the absorption maximum of **Az-BSQ-D** (λ_{cal} = 828 nm) was blue-shifted compared to that of **Az-BSQ-S** (λ_{cal} = 875 nm).

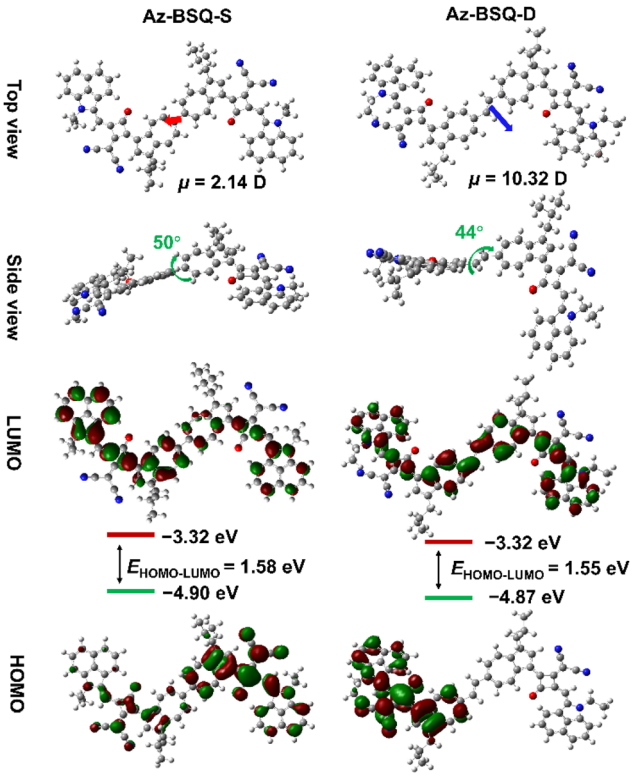

Fig. 2 Optimized molecular geometries, dipole moments, frontier molecular orbitals, and energy diagram of **Az-BSQ-S** and **Az-BSQ-D**.

Optical and electrochemical properties

The photophysical properties of three target compounds were investigated through UV-vis/NIR absorption spectrum and fluorescence spectrum. As shown in Fig. 3a, **Az-SQ** demon-

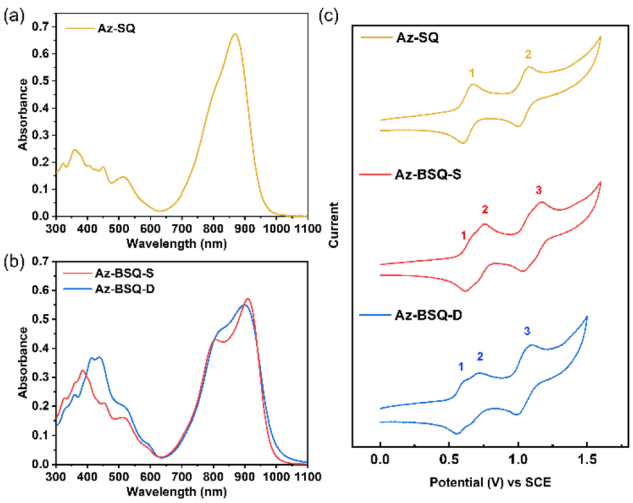

Fig. 3 UV-vis/NIR absorption spectra of (a) **Az-SQ** (10^{-5} M) and (b) **Az-BSQ-S** and **Az-BSQ-D** (5×10^{-6} M) in THF. (c) Cyclic voltammetry curves of **Az-SQ**, **Az-BSQ-S** and **Az-BSQ-D** in DCM ($TBAPF_6$ was used as the supporting electrolyte and SCE as the reference electrode) in the positive voltage range.

Table 1 Optical and electrochemical data of **Az-SQ**, **Az-BSQ-S** and **Az-BSQ-D**

Compound	λ_{max} (nm)	E_g^{opt} [a] (eV)	E_{ox1}^{onset} (V)	E_{red1}^{onset} (V)	E_{HOMO} [b] (eV)	E_{LUMO} [c] (eV)	E_g^{CV} [d] (eV)	E_g^{DFT} [e] (eV)
Az-SQ	868	1.31	0.58	−0.54	−4.98	−3.86	1.12	1.61
Az-BSQ-S	910	1.27	0.57	−0.52	−4.97	−3.88	1.09	1.58
Az-BSQ-D	900	1.26	0.53	−0.56	−4.93	−3.84	1.09	1.55

[a] Obtained from onset absorption wavelength (λ_{onset}) using the formula $E_g^{opt} = 1240/\lambda_{onset}$. [b] Calculated from $E_{HOMO} = -4.40 - E_{ox1}^{onset}$. [c] Calculated from $E_{LUMO} = -4.40 - E_{red1}^{onset}$. [d] Obtained from the equation $E_g^{CV} = E_{LUMO} - E_{HOMO}$. [e] Obtained from DFT calculations.

strated a unimodal peak in the near-infrared region, and its maximum absorption wavelength (λ_{max}) in tetrahydrofuran (THF) was centered at 868 nm with a molar extinction coefficient (ε_{max}) of 6.4 × 10^4 M^{-1} cm^{-1}. Distinct from **Az-SQ**, the absorption bands of **Az-BSQ-S** and **Az-BSQ-D** in the NIR region both presented a maximum absorption peak at 910 and 900 nm (ε_{max}: ~1.1 × 10^5 M^{-1} cm^{-1}), as well as a shoulder peak at 805 and 826 nm, respectively (Fig. 3b). Thus, compared with λ_{max} of **Az-SQ**, λ_{max} of **Az-BSQ-S** and **Az-BSQ-D** was bathochromically shifted by 42 nm and 32 nm, respectively, manifesting the intramolecular exciton coupling effect between the adjacent squaraine units.[41] The relative absorption maxima values were consistent with the TD-DFT calculation results. Moreover, both bis(squaraine) dyes showed negligible fluorescence in the NIR region due to the existence of azulene units (Fig. S3†).[21]

Cyclic voltammetry experiments were conducted in dichloromethane solutions with tetrabutylammonium hexafluorophosphate ($TBAPF_6$) as the supporting electrolyte and a saturated calomel electrode (SCE) as the reference electrode. As illustrated in Fig. 3c, **Az-SQ** presented two reversible oxidation peaks in the positive voltage range, while for **Az-BSQ-S** and **Az-BSQ-D**, the first reversible oxidation peaks were split into two peaks. This feature was also observed in the differential pulse voltammetry curves (Fig. S4†). This phenomenon could be regarded as the proof of intramolecular exciton coupling, which was also called the Davydov splitting.[18] Moreover, as shown in Table 1, the first onset oxidation potential (E_{ox1}^{onset} *vs.* SCE) of **Az-SQ**, **Az-BSQ-S** and **Az-BSQ-D** was 0.58, 0.57 and 0.53 V through referring to Fig. S5,† respectively. The first onset reduction potential (E_{red1}^{onset} *vs.* SCE) was −0.54, −0.52 and −0.56 V, respectively. Since the half-wave potential of the ferrocene/ferrocenium redox couple was measured to be 0.40 V under the same conditions and the energy level of ferrocene *versus* vacuum level was reported to be −4.8 eV,[42] the HOMO/LUMO energy levels of three compounds were calculated from the equation $E_{HOMO/LUMO} = -4.40 - E_{ox1/red1}^{onset}$. As a result, the E_{HOMO}/E_{LUMO} values of **Az-SQ**, **Az-BSQ-S** and **Az-BSQ-D** were −4.98 eV/−3.86 eV, −4.97 eV/−3.88 eV and −4.93 eV/−3.84 eV, respectively. The energy band gaps of the two bis(squaraine) dyes (1.09 eV) were close to the one of monomer (1.12 eV), which might be explained by the large torsional angles and inhomogeneous electron density distributions between monomeric squaraine moieties.[43] In addition, the absolute values of HOMO energy levels of **Az-BSQ-S** and **Az-BSQ-D** were close to the work function of gold metal (5.1 eV), so that they might be applied in the organic field-effect transistors (OFET) with Au as source/drain electrodes. Considering their HOMO and LUMO energy levels, both dimeric compounds are candidates for ambipolar organic semiconductor materials.[44]

Aggregation behavior studies

Az-BSQ-S and **Az-BSQ-D** possessed different dipole moments and directions, which could result in distinct molecular aggregates.[45] Besides, the self-assembly behavior could be adjusted by changing solvents, the concentration of compounds, temperatures, *etc.*[46] Generally, when dyes are aligned in a slip-stacked way, J-type aggregates are formed and their maximum absorption wavelengths will be bathochromically shifted relative to the molecular state. When dyes are packed co-facially, H-type aggregates are formed and their λ_{max} will be hypsochromically shifted compared with those of molecular state.[47]

First, the aggregation behavior studies were conducted in the THF/H_2O mixed solvents.[48] As demonstrated in Fig. 4a, when the water volume fraction (f_{water}) was 10%, the maximum absorption peak of **Az-BSQ-S** was located at 887 nm and accompanied by a shoulder peak at 798 nm. When f_{water} achieved 40%, a new peak at 676 nm appeared. With the water volume ratio increasing constantly, the intensity of the absorption peaks at the long-wavelength gradually got weakened and the peak at 676 nm turned to be the maximum absorption

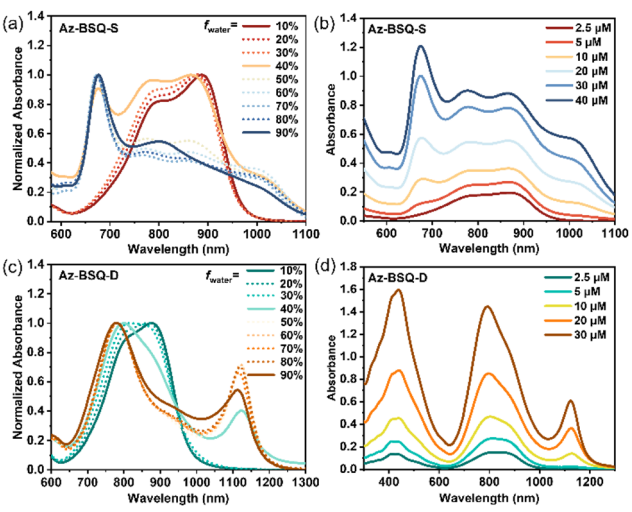

Fig. 4 Absorption spectra of (a) **Az-BSQ-S** and (c) **Az-BSQ-D** (10 μM) in THF/H_2O solvents with f_{water} ranging from 10% to 90%. Absorption spectra of (b) **Az-BSQ-S** and (d) **Az-BSQ-D** with different concentrations in THF/H_2O mixed solvents (f_{water} = 40%).

peak, indicating the existence of H-aggregates.[49] Furthermore, the variations in the concentration-dependent absorption spectra of **Az-BSQ-S** (Fig. 4b) were examined in the THF/H_2O mixtures (f_{water} = 40%).[50] When the concentration of **Az-BSQ-S** was as low as 2.5 μM, its absorption band in the vis-NIR region included two peaks at 868 nm and 747 nm. As the concentration increased to 5 μM and beyond, a new peak at 676 nm was observed and it was gradually magnified with the increase in concentrations. As shown in Fig. S6a,† the absorbance ratio of two peaks at 676 nm and 868 nm (A_{676}/A_{868}) was substantially increased from 0.23 to 1.27. Moreover, a shoulder peak located at 1010 nm came into existence at a compound concentration of 10 μM. Eventually, the maximum absorption wavelength of **Az-BSQ-S** (50 μM) turned out to be 676 nm, which was hypsochromically shifted by 234 nm relative to the one in pure THF solutions. In addition, the transmission electron microscopic (TEM) images revealed the morphology of aggregates (10 μM, f_{water} = 90%) to be nanoparticles (Fig. S7a†), dynamic light scattering (DLS) experiments indicated that the average diameter of the nanoparticles was about 60 nm and the polydispersity index (PDI) was about 0.29 (Fig. S7b†). The above-mentioned data confirmed that **Az-BSQ-S** was inclined to form H-aggregate nanoparticles in the THF/H_2O system.

The aggregation behavior studies of **Az-BSQ-D** were conducted in a similar manner. As shown in Fig. 4c, when the water volume ratio was 10%, the maximum absorption wavelength of **Az-BSQ-D** was about 876 nm. As the water content increased, the absorption band was hypsochromically shifted. Then, dramatic spectrum changes occurred at a water content of 40%, where λ_{max} of **Az-BSQ-D** was centered at 800 nm and a new NIR-II absorption peak appeared at 1092 nm. Two possible reasons could lead to the emergence of the red-shifted absorption band. On the one hand, there were some J-aggregates except for the dominant H-aggregates.[51,52] On the other hand, the intermolecular charge transfer effect in the densely packed H-aggregates caused the long-wavelength absorption.[12,13] Besides, we recorded the spectra of **Az-BSQ-D** with different concentrations in the THF/H_2O (f_{water} = 40%) system (Fig. 4d). The peak absorbance ratios of 795 nm *versus* 868 nm (A_{795}/A_{868}) experienced exponential growth with the increase in concentrations (Fig. S6b†), suggesting the formation of H-aggregates. In addition, the high concentrations (≥10 μM) also facilitated the appearance of NIR-II absorption bands. Analogically, TEM and DLS characterizations (Fig. S7c and d†) depicted **Az-BSQ-D** aggregates (10 μM, f_{water} = 90%) as nanoparticles with an average width of 95 nm (PDI = 0.20).

Then, the self-assembly process under the influence of temperature[53,54] was studied through the absorption spectra in the THF/H_2O mixed solvents (10 μM, f_{water} = 90%). For **Az-BSQ-S** (Fig. S8a†), two peaks were selected to trace their absorbance variations during the heating process: one is correlated with H-aggregates (λ = 676 nm), and the other one corresponds to the molecular state at low concentrations and water contents (λ = 868 nm). The peak intensity at 676 nm gradually decreased and ultimately diminished at 60 °C, while the peak intensity at 868 nm increased consistently. It pointed out that the H-aggregates underwent the dissociation process.[55] For **Az-BSQ-D**, the absorbance variation tendency of two wavelengths was also recorded (Fig. S8b†). The descent of the absorbance peak at 1125 nm also implied the disaggregation course. Therefore, **Az-BSQ-S** and **Az-BSQ-D** aggregates were thermal responsive.[56]

Apart from the polar protic solvent, hexane is a kind of nonpolar poor solvent for squaraine dyes. The properties of **Az-BSQ-S** and **Az-BSQ-D** aggregates were then studied in the THF/hexane system.[57] As shown in Fig. 5a, upon increasing the hexane volume fraction (f_{hexane}) from 10% to 80%, the maximum absorption peak of **Az-BSQ-S** was blue-shifted from 910 nm to 805 nm, indicating the formation of H-aggregates. However, great changes were observed in the absorption spectrum at f_{hexane} of 90%, where the maximum absorption peak was centered at 978 nm, demonstrating the J-aggregate feature. Meanwhile, the morphology of the nanosheet with a length of about 600 nm and a width of about 220 nm was determined from the TEM images (Fig. S9a†), and these nanosheets can further agglomerate into nanoflowers. In other words, the appearance of J-aggregate nanosheets triggered substantial changes in the absorption spectrum.[58,59]

Furthermore, the absorbance variations of **Az-BSQ-S** with different concentrations in THF/hexane (f_{hexane} = 60%) were recorded, and are presented in Fig. 5b and Fig. S10a.† Two main absorption peaks located at about 925 nm and 795 nm were labeled as "0–0" and "0–1" peaks, respectively.[60] With the increase in concentration from 2.5 μM to 40 μM, the peak absorbance ratio (A_{0-0}/A_{0-1}) was lowered cooperatively from 1.16 (>1) to 0.84 (<1), which could be regarded as the charac-

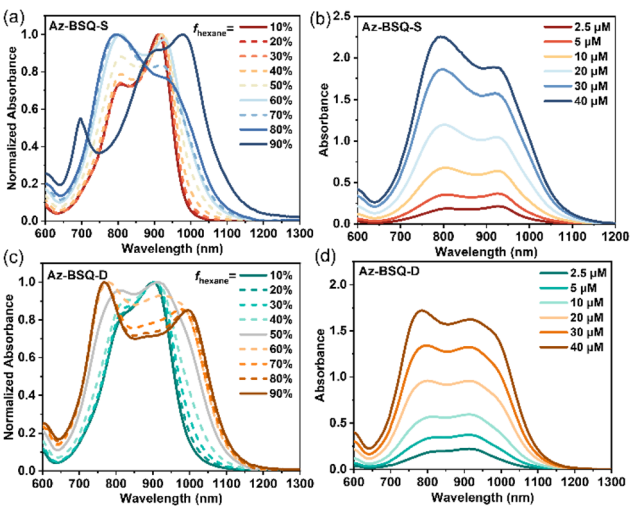

Fig. 5 Normalized absorption spectra of (a) **Az-BSQ-S** and (c) **Az-BSQ-D** (10 μM) in THF/hexane mixed solvents with hexane volume fractions ranging from 10% to 90%. Absorption spectra of (b) **Az-BSQ-S** (f_{hexane} = 60%) and (d) **Az-BSQ-D** (f_{hexane} = 50%) at different concentrations in the THF/hexane system.

teristic feature of H-aggregation.[61] Additionally, the concentration-dependent spectra demonstrated the analogous variation tendency with the hexane contents increasing from 10% to 80%.

For **Az-BSQ-D**, when the volume fraction of hexane was as high as 90%, the main absorbance band was separated into two peaks located at 768 nm and 995 nm (Fig. 5c), which were respectively red-shifted by 95 nm and blue-shifted by 132 nm relative to the maximum absorbance wavelength in pure THF. This again indicated the co-existence of two types of aggregates or ICT effect, which agreed well with the aggregation modes of **Az-BSQ-D** in the THF/H_2O system. Then, from the concentration-dependent absorption spectra (Fig. 5d), the absorbance ratio changing plots of two main peaks (A_{0-0}/A_{0-1}) are illustrated in Fig. S10b.† The value decreased in a sigmoidal shape, indicative of the occurrence of isodesmic H-aggregates with f_{hexane} of 50%.[62] Besides, as shown in Fig. S9c,† **Az-BSQ-D** could hardly form nanosheets or discrete nanostructures in THF/hexane mixed solvents (10 μM, f_{hexane} = 90%), which was distinguished from **Az-BSQ-S**.

Moreover, the temperature-dependent self-assembly behaviors of **Az-BSQ-S** and **Az-BSQ-D** in the THF/hexane (f_{hexane} = 60%) system were investigated in a similar manner (Fig. 6 and Fig. S11†). Both compounds showed two isosbestic points in different spectra,[20,63] suggesting that there were only two species in the dispersions and the aggregate was directly transformed into free molecules upon heating. More importantly, we could exclude the existence of J-aggregates for **Az-BSQ-D** and the emerging red-shifted absorption peak could be mainly ascribed to the ICT effect. Besides, as demonstrated in Fig. 6b and d, the spectrum of **Az-BSQ-S** or **Az-BSQ-D** at room temperature was almost overlapped with the one obtained after slowly cooling to room temperature, evidencing that the aggregate structures formed at high temperatures would spontaneously convert into thermodynamically stable H-aggregates at room temperature. All these experiment results verified that the self-assembly behaviors of azulene-bridged bis(squaraine) dyes could be affected through the modification of connection model and surrounding environments.

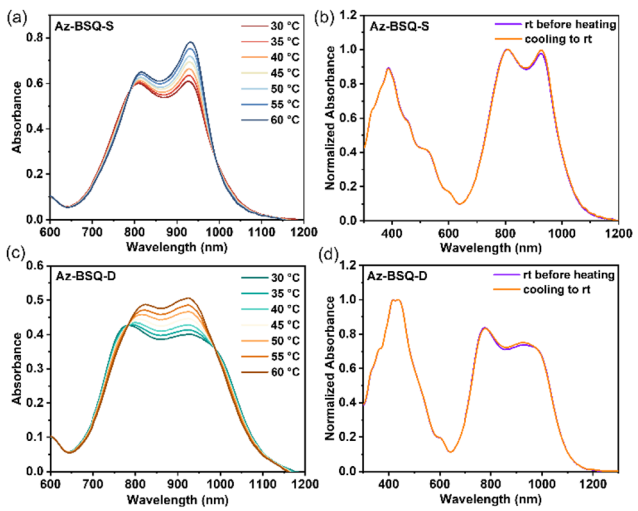

Fig. 6 Temperature-dependent absorption spectra of (a) **Az-BSQ-S** and (c) **Az-BSQ-D** during the heating process in the THF/hexane system (10 μM, f_{hexane} = 60%). Absorption spectra of (b) **Az-BSQ-S** and (d) **Az-BSQ-D** before heating and after cooling to room temperature.

In addition to the impact of connection model, the effects of dimerization on film aggregate properties were evaluated. OFET devices based on **Az-SQ**, **Az-BSQ-S** and **Az-BSQ-D** were constructed with thermally evaporated gold as the top electrode. Moreover, the thermal annealing could induce the rearrangement of molecular aggregates in films,[64] thermal gravity analysis (TGA) revealed that **Az-SQ** possessed better thermal stability than the other two dimer compounds and **Az-BSQ-S** gradually decomposed above 120 °C (Fig. S12†). Therefore, the OFET devices were heated at 80 °C for 30 min and cooled slowly to room temperature in a nitrogen atmosphere. Typical transfer and output curves are demonstrated in Fig. S13–S15,† and the corresponding OFET device performance values are listed in Table S1.† **Az-SQ** films did not exhibit typical I_{DS}–V_G slopes before thermal treatment but demonstrated p-type OFET characteristics after thermal annealing at 80 °C, where the average hole mobility was calculated to be about 3×10^{-3} cm^2 V^{-1} s^{-1} in the saturated regime, the gate voltage was about −19 V and the on/off ratio was as high as 10^6. Furthermore, both bis(squaraine) films-based OFET devices presented ambipolar carrier transport properties, with the average electron and hole transport mobility being 2.5×10^{-4} cm^2 V^{-1} s^{-1} and 1.0×10^{-4} cm^2 V^{-1} s^{-1} (for **Az-BSQ-S**), and 1.3×10^{-4} cm^2 V^{-1} s^{-1} and 1.3×10^{-4} cm^2 V^{-1} s^{-1} (for **Az-BSQ-D**), respectively. The ambipolar OFET characteristics of two dimeric compounds might be correlated with their high HOMO and low LUMO energy levels as well as longer conjugation lengths and peculiar electron distribution modes. On the contrary, the thermal treatment has negligible influence on the OFET performance for these two bis(squaraine) dyes, and their hole and electron mobilities were monitored around the order of 10^{-4} cm^2 V^{-1} s^{-1}. To sum up, the dimerization of conjugated molecules could affect the charge transport properties and the thermal responsiveness of the molecular aggregates.

Then, to gain insights into the effect of thermal annealing, atom force microscopic (AFM) images of three films were acquired (Fig. 7). Morphological changes occurred in **Az-SQ** films. The roughness root mean square (RMS) value was increased from 0.24 nm to 1.0 nm and small-sized granular domains were observed in the 80 °C-annealed thin films. However, the film surface based on **Az-BSQ-S** and **Az-BSQ-D** experienced a little variation upon thermal annealing with the RMS values around 0.24 nm. These findings were consistent with the OFET device performance. Moreover, as exhibited in Fig. S16,† the absorption spectrum of **Az-SQ** film was blue-shifted by about 100 nm after the thermal treatment, verifying the transformation of molecular packing. These results indicated that the **Az-SQ** film aggregates were reorganized to the aggregate structures more suitable for charge transport.[65]

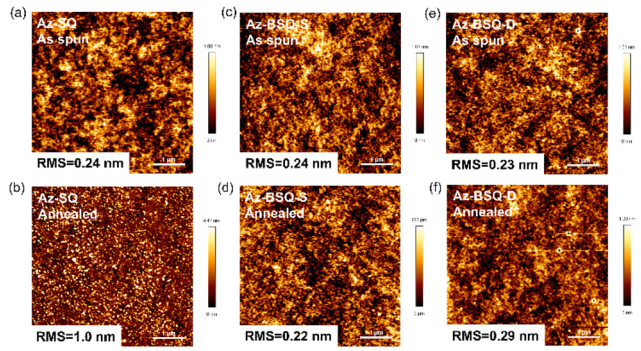

Fig. 7 AFM images of (a, b) **Az-SQ**, (c, d) **Az-BSQ-S** and (e, f) **Az-BSQ-D** films before and after thermal annealing at 80 °C.

Conclusions

In conclusion, azulenyl squaraine **Az-SQ** containing a benz[*cd*] indolium unit has been designed, and then directly linked and vinylene-bridged bis(squaraine) dyes **Az-BSQ-S** and **Az-BSQ-D** with an azulene core have been synthesized. Both bis(squaraine) compounds exhibited a maximum absorption wavelength beyond 900 nm and narrow HOMO–LUMO band gaps as nearly as 1.0 eV. Two dimeric molecules demonstrated aggregate polymorphisms. **Az-BSQ-S** was inclined to form the packing structures dominated by H-aggregates. Meanwhile, it could be transformed into J-type aggregated nanosheets in the binary solvents of THF and hexane. Besides, the absorption spectra of **Az-BSQ-D** manifested the ICT effect in H-aggregates. Furthermore, the conjugation of azulenyl squaraines affects the carrier transport properties as well as the thermal responsiveness of films. Therefore, our work has enriched the compound library of bis(squaraine) dyes and suggests that the connection model of monomeric units has significant effects on the self-assembly behaviors, which deserve great attention during the structural modification of functional molecules.

Author contributions

Y. Yao: conceptualization, investigation, methodology, writing – original draft; H. Lin: software; S. Cai: investigation; X. Yang: software, project administration; X. Gao: conceptualization, funding acquisition, supervision, writing – review & editing.

Data availability

The data supporting this article have been included as part of the ESI.†

Conflicts of interest

There are no conflicts to declare.

Acknowledgements

This work was supported by the National Natural Science Foundation of China (no. 22225506), the Strategic Priority Research Program of the Chinese Academy of Sciences (grant no. XDB0610000).

References

1 Z. Liu, Y. Wu, Q. Zhang and X. Gao, Non-fullerene small molecule acceptors based on perylene diimides, *J. Mater. Chem. A*, 2016, **4**, 17604–17622.
2 M. A. Rajora, J. W. H. Lou and G. Zheng, Advancing porphyrin's biomedical utility via supramolecular chemistry, *Chem. Soc. Rev.*, 2017, **46**, 6433–6469.
3 S. Sreejith, P. Carol, P. Chithra and A. Ajayaghosh, Squaraine dyes: a mine of molecular materials, *J. Mater. Chem.*, 2008, **18**, 264–274.
4 A. Ajayaghosh, P. Chithra, R. Varghese and K. P. Divya, Controlled self-assembly of squaraines to 1D supramolecular architectures with high molar absorptivity, *Chem. Commun.*, 2008, 969–971.
5 Z. Yan, S. Guang, H. Xu, X. Su, X. Ji and X. Liu, Supramolecular self-assembly structures and properties of zwitterionic squaraine molecules, *RSC Adv.*, 2013, **3**, 8021–8027.
6 A. K. Singh, M. F. M. Kavungathodi, A. J. Mozer, K. Krishnamoorthy and J. Nithyanandhan, Solvent-Dependent Functional Aggregates of Unsymmetrical Squaraine Dyes on TiO2 Surface for Dye-Sensitized Solar Cells, *Langmuir*, 2022, **38**, 14808–14818.
7 D. Zhang, Y. X. Zhao, Z. Y. Qiao, U. Mayerhoffer, P. Spenst, X. J. Li, F. Würthner and H. Wang, Nano-confined squaraine dye assemblies: new photoacoustic and near-infrared fluorescence dual-modular imaging probes in vivo, *Bioconjugate Chem.*, 2014, **25**, 2021–2029.
8 C.-A. Shen, M. Stolte, J. H. Kim, A. Rausch and F. Würthner, Double J-Coupling Strategy for Near Infrared Emitters, *J. Am. Chem. Soc.*, 2021, **143**, 11946–11950.
9 C.-A. Shen and F. Würthner, NIR-emitting squaraine J-aggregate nanosheets, *Chem. Commun.*, 2020, **56**, 9878–9881.
10 E. E. Jelley, Molecular, Nematic and Crystal States of I: I'-Diethyl-ψ-Cyanine Chloride, *Nature*, 1937, **139**, 631–632.
11 M. Kasha, H. R. Rawls and M. Ashraf El-Bayoumi, The exciton model in molecular spectroscopy, *Pure Appl. Chem.*, 1965, **11**, 371–392.
12 J. H. Kim, A. Liess, M. Stolte, A. M. Krause, V. Stepanenko, C. Zhong, D. Bialas, F. Spano and F. Würthner, An Efficient Narrowband Near–Infrared at 1040 nm Organic Photodetector Realized by Intermolecular Charge Transfer Mediated Coupling Based on a Squaraine Dye, *Adv. Mater.*, 2021, **33**, 2100582.
13 N. J. Hestand, C. Zheng, A. R. Penmetcha, B. Cona, J. A. Cody, F. C. Spano and C. J. Collison, Confirmation of

the Origins of Panchromatic Spectra in Squaraine Thin Films Targeted for Organic Photovoltaic Devices, *J. Phys. Chem. C*, 2015, **119**, 18964–18974.

14 D. Yang, H. Sasabe, T. Sano and J. Kido, Low-Band-Gap Small Molecule for Efficient Organic Solar Cells with a Low Energy Loss below 0.6 eV and a High Open-Circuit Voltage of over 0.9 V, *ACS Energy Lett.*, 2017, **2**, 2021–2025.

15 D. Yang, H. Sasabe, Y. Jiao, T. Zhuang, Y. Huang, X. Pu, T. Sano, Z. Lu and J. Kido, An effective pi-extended squaraine for solution-processed organic solar cells with high efficiency, *J. Mater. Chem. A*, 2016, **4**, 18931–18941.

16 E. Michail, M. H. Schreck, M. Holzapfel and C. Lambert, Exciton coupling effects on the two-photon absorption of squaraine homodimers with varying bridge units, *Phys. Chem. Chem. Phys.*, 2020, **22**, 18340–18350.

17 X. Wang, Z. Jiang, Z. Liang, T. Wang, Y. Chen and Z. Liu, Discovery of BODIPY J-aggregates with absorption maxima beyond 1200 nm for biophotonics, *Sci. Adv.*, 2020, **8**, eadd5660.

18 X. Guo, J. Yang, M. Li, F. Zhang, W. Bu, H. Li, Q. Wu, D. Yin, L. Jiao and E. Hao, Unique Double Intramolecular and Intermolecular Exciton Coupling in Ethene–Bridged aza–BODIPY Dimers for High–Efficiency Near–Infrared Photothermal Conversion and Therapy, *Angew. Chem., Int. Ed.*, 2022, **61**, e202211081.

19 H. Ceymann, A. Rosspeintner, M. H. Schreck, C. Mützel, A. Stoy, E. Vauthey and C. Lambert, Cooperative enhancement versus additivity of two-photon-absorption cross sections in linear and branched squaraine superchromophores, *Phys. Chem. Chem. Phys.*, 2016, **18**, 16404–16413.

20 C. A. Shen, D. Bialas, M. Hecht, V. Stepanenko, K. Sugiyasu and F. Würthner, Polymorphism in Squaraine Dye Aggregates by Self–Assembly Pathway Differentiation: Panchromatic Tubular Dye Nanorods versus J–Aggregate Nanosheets, *Angew. Chem., Int. Ed.*, 2021, **60**, 11949–11958.

21 H. Xin, B. Hou and X. Gao, Azulene-Based pi-Functional Materials: Design, Synthesis, and Applications, *Acc. Chem. Res.*, 2021, **54**, 1737–1753.

22 Y. Yamaguchi, M. Takubo, K. Ogawa, K.-I. Nakayama, T. Koganezawa and H. Katagiri, Terazulene Isomers: Polarity Change of OFETs through Molecular Orbital Distribution Contrast, *J. Am. Chem. Soc.*, 2016, **138**, 11335–11343.

23 Y. Shibuya, A. Matsunaga, D. Kumaki, S. Tokito and H. Katagiri, Azulene End-Capped 1,3,4-Thiadiazole as an n-Type Organic Semiconductor with a Herringbone–Brickwork Cooperative 2D Layered Structure, *Cryst. Growth Des.*, 2022, **22**, 6554–6563.

24 H. Gao, Y. Yao, C. Li, J. Zhang, H. Yu, X. Yang, J. Shen, Q. Liu, R. Xu, X. Gao and D. Ding, Concentrating Excited State Energy on Non–Radiative Decay Pathways with Fused Azulenyl Squaraine Derivatives for Improving Second Near–Infrared Phototheranostics, *Angew. Chem., Int. Ed.*, 2024, **63**, e202400372.

25 E. C. P. Smits, S. Setayesh, T. D. Anthopoulos, M. Buechel, W. Nijssen, R. Coehoorn, P. W. M. Blom, B. de Boer and D. M. de Leeuw, Near-infrared light-emitting ambipolar organic field-effect transistors, *Adv. Mater.*, 2007, **19**, 734–738.

26 W. Cao and E. M. Sletten, Fluorescent Cyanine Dye J-Aggregates in the Fluorous Phase, *J. Am. Chem. Soc.*, 2018, **140**, 2727–2730.

27 H. Chen, W. Zhang, S. Ren, X. Zhao, Y. Jiao, Y. Wang, J. F. Stoddart and X. Guo, Temperature–Triggered Supramolecular Assembly of Organic Semiconductors, *Adv. Mater.*, 2021, **34**, 2101487.

28 X. Ma, Y. Huang, W. Chen, J. Liu, S. H. Liu, J. Yin and G. F. Yang, J–Aggregates Formed by NaCl Treatment of Aza–Coating Heptamethine Cyanines and Their Application to Monitoring Salt Stress of Plants and Promoting Photothermal Therapy of Tumors, *Angew. Chem., Int. Ed.*, 2022, **62**, e202216109.

29 K. Strassel, A. Kaiser, S. Jenatsch, A. C. Veron, S. B. Anantharaman, E. Hack, M. Diethelm, F. Nuesch, R. Aderne, C. Legnani, S. Yakunin, M. Cremona and R. Hany, Squaraine Dye for a Visibly Transparent All-Organic Optical Upconversion Device with Sensitivity at 1000 nm, *ACS Appl. Mater. Interfaces*, 2018, **10**, 11063–11069.

30 B. Li, L. Lu, M. Zhao, Z. Lei and F. Zhang, An Efficient 1064 nm NIR-II Excitation Fluorescent Molecular Dye for Deep-Tissue High-Resolution Dynamic Bioimaging, *Angew. Chem., Int. Ed.*, 2018, **57**, 7483–7487.

31 B. Hou, Z. Zhou, C. Yu, X.-S. Xue, J. Zhang, X. Yang, J. Li, C. Ge, J. Wang and X. Gao, 2,6-Azulene-based Homopolymers: Design, Synthesis, and Application in Proton Exchange Membrane Fuel Cells, *ACS Macro Lett.*, 2022, **11**, 680–686.

32 S. So, H. Choi, H. Min Ko, C. Kim, S. Paek, N. Cho, K. Song, J. K. Lee and J. Ko, Novel unsymmetrical push–pull squaraine chromophores for solution processed small molecule bulk heterojunction solar cells, *Sol. Energy Mater. Sol. Cells*, 2012, **98**, 224–232.

33 H. Wang, C. Cao, H. Chen, H. Lai, C. Ke, Y. Zhu, H. Li and F. He, Oligomeric Acceptor: A "Two–in–One" Strategy to Bridge Small Molecules and Polymers for Stable Solar Devices, *Angew. Chem., Int. Ed.*, 2022, **61**, e202201844.

34 Y. Asanuma, H. Mori, R. Takahashi and Y. Nishihara, Vinylene-bridged difluorobenzo[c][1,2,5]-thiadiazole (FBTzE): a new electron-deficient building block for high-performance semiconducting polymers in organic electronics, *J. Mater. Chem. C*, 2019, **7**, 905–916.

35 M. Odagi, T. Matoba, K. Hosoya and K. Nagasawa, Enantioselective Total Synthesis of (+)-Stephadiamine through Bioinspired Aza-Benzilic Acid Type Rearrangement, *J. Am. Chem. Soc.*, 2021, **143**, 2699–2704.

36 Y. Zhu, Z. Xia, Z. Cai, Z. Yuan, N. Jiang, T. Li, Y. Wang, X. Guo, Z. Li, S. Ma, D. Zhong, Y. Li and J. Wang, Synthesis and Characterization of Hexapole [7]Helicene, A Circularly Twisted Chiral Nanographene, *J. Am. Chem. Soc.*, 2018, **140**, 4222–4226.

37 Y. Hu, Z. Wang, X. Zhang, X. Yang, C. Ge, L. Fu and X. Gao, A Class of Electron-Transporting Vinylogous Tetrathiafulvalenes Constructed by the Dimerization of Core-Expanded Naphthalenediimides, *Org. Lett.*, 2017, **19**, 468–471.

38 M. J. Frisch, G. W. Trucks, H. B. Schlegel, G. E. Scuseria, M. A. Robb, J. R. Cheeseman, G. Scalmani, V. Barone, G. A. Petersson, H. Nakatsuji, X. Li, M. Caricato, A. V. Marenich, J. Bloino, B. G. Janesko, R. Gomperts, B. Mennucci, H. P. Hratchian, J. V. Ortiz, A. F. Izmaylov, J. L. Sonnenberg, D. Williams-Young, F. Ding, F. Lipparini, F. Egidi, J. Goings, B. Peng, A. Petrone, T. Henderson, D. Ranasinghe, V. G. Zakrzewski, J. Gao, N. Rega, G. Zheng, W. Liang, M. Hada, M. Ehara, K. Toyota, R. Fukuda, J. Hasegawa, M. Ishida, T. Nakajima, Y. Honda, O. Kitao, H. Nakai, T. Vreven, K. Throssell, J. A. Montgomery Jr., J. E. Peralta, F. Ogliaro, M. J. Bearpark, J. J. Heyd, E. N. Brothers, K. N. Kudin, V. N. Staroverov, T. A. Keith, R. Kobayashi, J. Normand, K. Raghavachari, A. P. Rendell, J. C. Burant, S. S. Iyengar, J. Tomasi, M. Cossi, J. M. Millam, M. Klene, C. Adamo, R. Cammi, J. W. Ochterski, R. L. Martin, K. Morokuma, O. Farkas, J. B. Foresman and D. J. Fox, *Gaussian 16 Rev. B.01*, 2016.

39 J. Wu, D. Yang, Q. Wang, L. Yang, H. Sasabe, T. Sano, J. Kido, Z. Lu and Y. Huang, Central dicyanomethylene-substituted unsymmetrical squaraines and their application in organic solar cells, *J. Mater. Chem. A*, 2018, **6**, 5797–5806.

40 Y. Guo, Y. Li, O. Awartani, J. Zhao, H. Han, H. Ade, D. Zhao and H. Yan, A Vinylene–Bridged Perylenediimide–Based Polymeric Acceptor Enabling Efficient All–Polymer Solar Cells Processed under Ambient Conditions, *Adv. Mater.*, 2016, **28**, 8483–8489.

41 E. Michail, M. H. Schreck, L. Wittmann, M. Holzapfel and C. Lambert, Enhanced Two–Photon Absorption and Promising Broad Energy Range Optical Power Limiting Properties of Transoid and Cisoid Benzodipyrrolenine-Fused Squaraine Dimers, *Chem. Mater.*, 2021, **33**, 3121–3131.

42 Y. Liu, M. S. Liu and A. K. Y. Jen, Synthesis and characterization of a novel and highly efficient light-emitting polymer, *Acta Polym.*, 1999, **50**, 105–108.

43 S. Kuster and T. Geiger, Strategies and investigations on bridging squaraine dye units, *Dyes Pigm.*, 2012, **95**, 657–670.

44 T. Higashino and T. Mori, Small-molecule ambipolar transistors, *Phys. Chem. Chem. Phys.*, 2022, **24**, 9770–9806.

45 D. Bialas, E. Kirchner, M. I. S. Roehr and F. Würthner, Perspectives in Dye Chemistry: A Rational Approach toward Functional Materials by Understanding the Aggregate State, *J. Am. Chem. Soc.*, 2021, **143**, 4500–4518.

46 M. F. J. Mabesoone, A. R. A. Palmans and E. W. Meijer, Solute–Solvent Interactions in Modern Physical Organic Chemistry: Supramolecular Polymers as a Muse, *J. Am. Chem. Soc.*, 2020, **142**, 19781–19798.

47 Q. Liao, Q. Li and Z. Li, The Key Role of Molecular Packing in Luminescence Property: From Adjacent Molecules to Molecular Aggregates, *Adv. Mater.*, 2023, DOI: **10.1002/adma.202306617**.

48 Y. Yao, X. Sun, Z. Zhang, H. Yu, X. Yang, D. Ding and X. Gao, Azulene-Containing Bis(squaraine) Dyes: Design, Synthesis and Aggregation Behaviors, *Chem. – Eur. J.*, 2024, **30**, e202400474.

49 A. Zitzler-Kunkel, M. R. Lenze, K. Meerholz and F. Würthner, Enhanced photocurrent generation by folding-driven H-aggregate formation, *Chem. Sci.*, 2013, **4**, 2071–2075.

50 K. Cai, J. Xie, D. Zhang, W. Shi, Q. Yan and D. Zhao, Concurrent Cooperative J-Aggregates and Anticooperative H-Aggregates, *J. Am. Chem. Soc.*, 2018, **140**, 5764–5773.

51 G. M. Paternò, L. Moretti, A. J. Barker, C. D'Andrea, A. Luzio, N. Barbero, S. Galliano, C. Barolo, G. Lanzani and F. Scotognella, Near-infrared emitting single squaraine dye aggregates with large Stokes shifts, *J. Mater. Chem. C*, 2017, **5**, 7732–7738.

52 F.-F. An, Z.-J. Deng, J. Ye, J.-F. Zhang, Y.-L. Yang, C.-H. Li, C.-J. Zheng and X.-H. Zhang, Aggregation-Induced Near-Infrared Absorption of Squaraine Dye in an Albumin Nanocomplex for Photoacoustic Tomography in Vivo, *ACS Appl. Mater. Interfaces*, 2014, **6**, 17985–17992.

53 Z. Chen, P. Cai, J. Chen, X. Liu, L. Zhang, L. Lan, J. Peng, Y. Ma and Y. Cao, Low band-gap conjugated polymers with strong interchain aggregation and very high hole mobility towards highly efficient thick-film polymer solar cells, *Adv. Mater.*, 2014, **26**, 2586–2591.

54 Y. Liu, J. Zhao, Z. Li, C. Mu, W. Ma, H. Hu, K. Jiang, H. Lin, H. Ade and H. Yan, Aggregation and morphology control enables multiple cases of high-efficiency polymer solar cells, *Nat. Commun.*, 2014, **5**, 5293.

55 W. Shi, R. Wei, D. Zhang, L. Meng, J. Xie, K. Cai and D. Zhao, Dual Cooperatively Grown J–aggregates with Different Nucleus Size, *Angew. Chem., Int. Ed.*, 2022, **61**, e202208635.

56 C. Yang, W. Zhang, X. Pang, F. Xiao, S. K. Kalva, Y. Zhang, M. Pramanik, L. Tian, G. Liu and M. Wang, Polyester–tethered near–infrared fluorophores confined in colloidal nanoparticles: Tunable and thermo-responsive aggregation and biomedical applications, *Aggregate*, 2022, **4**, e261.

57 X. Guo, W. Sheng, H. Pan, L. Guo, H. Zuo, Z. Wu, S. Ling, X. Jiang, Z. Chen, L. Jiao and E. Hao, Tuning Shortwave–Infrared J–aggregates of Aromatic Ring–Fused Aza–BODIPYs by Peripheral Substituents for Combined Photothermal and Photodynamic Therapies at Ultralow Laser Power, *Angew. Chem., Int. Ed.*, 2024, **63**, e202319875.

58 Y. Kubota, M. Nakazawa, J. Lee, R. Naoi, M. Tachikawa, T. Inuzuka, K. Funabiki, M. Matsui and T. Kim, Synthesis of near-infrared absorbing and fluorescent bis(pyrrol-2-yl) squaraines and their halochromic properties, *Org. Chem. Front.*, 2021, **8**, 6226–6243.

59 M. Hecht, P. Leowanawat, T. Gerlach, V. Stepanenko, M. Stolte, M. Lehmann and F. Würthner, Self–Sorting Supramolecular Polymerization: Helical and Lamellar Aggregates of Tetra–Bay–Acyloxy Perylene Bisimide, *Angew. Chem., Int. Ed.*, 2020, **59**, 17084–17090.

60 Y. Hong, F. Schlosser, W. Kim, F. Würthner and D. Kim, Ultrafast Symmetry-Breaking Charge Separation in a Perylene Bisimide Dimer Enabled by Vibronic Coupling and Breakdown of Adiabaticity, *J. Am. Chem. Soc.*, 2022, **144**, 15539–15548.

61 F. C. Spano, The Spectral Signatures of Frenkel Polarons in H- and J-Aggregates, *Acc. Chem. Res.*, 2010, **43**, 429–439.

62 M. M. J. Smulders, M. M. L. Nieuwenhuizen, T. F. A. de Greef, P. van der Schoot, A. P. H. J. Schenning and E. W. Meijer, How to Distinguish Isodesmic from Cooperative Supramolecular Polymerisation, *Chem. – Eur. J.*, 2009, **16**, 362–367.

63 M. Wehner, M. I. S. Röhr, M. Bühler, V. Stepanenko, W. Wagner and F. Würthner, Supramolecular Polymorphism in One-Dimensional Self-Assembly by Kinetic Pathway Control, *J. Am. Chem. Soc.*, 2019, **141**, 6092–6107.

64 G. Chen, H. Sasabe, W. Lu, X.-F. Wang, J. Kido, Z. Hong and Y. Yang, J-aggregation of a squaraine dye and its application in organic photovoltaic cells, *J. Mater. Chem. C*, 2013, **1**, 6547–6552.

65 H. Ran, F. Li, R. Zheng, H. Zhang, F. Xie, P. Jin, Z. Lei, X.-T. Wang and J.-Y. Hu, Polarity change of OFETs based on Dithienocoronene Diimide (DTCDI)-Derived isomeric triads end-capped with Azulene, *Dyes Pigm.*, 2022, **203**, 110311.

